NANO LETTERS

Letter

pubs.acs.org/NanoLett

Crystal Structure and Transport in Merged InAs Nanowires MBE Grown on (001) InAs

Jung-Hyun Kang,*[,†,⊥] Yonatan Cohen,[†,⊥] Yuval Ronen,[†,⊥] Moty Heiblum,[†] Ryszard Buczko,[§] Perla Kacman,[§] Ronit Popovitz-Biro,[‡] and Hadas Shtrikman[†]

[†]Braun Center for Submicron Research, Department of Condensed Matter Physics and [‡]Department of Chemical Research Support, Weizmann Institute of Science, Rehovot 76100, Israel

[§]Institute of Physics Polish Academy of Science, Al. Lotnikow 32/46, 02-668 Warsaw, Poland

Supporting Information

ABSTRACT: Molecular beam epitaxy growth of merging InAs nanowire intersections, that is, a first step toward the realization of a network of such nanowires, is reported. While InAs nanowires play already a leading role in the search for Majorana fermions, a network of these nanowires is expected to promote their exchange and allow for further development of this field. The structural properties of merged InAs nanowire intersections have been investigated using scanning and transmission electron microscope imaging. At the heart of the intersection, a sharp change of the crystal structure from wurtzite to perfect zinc blende is observed. The performed low-temperature conductance measurements demonstrate that the intersection does not impose an obstacle to current transport.

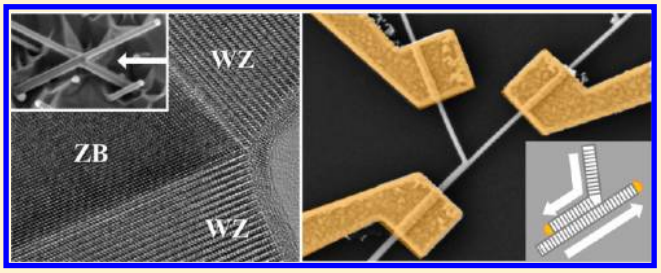

KEYWORDS: *InAs NWs, merging NW intersections, Y-shape, K-shape, wurtzite, zinc blende, Majorana fermions*

Semiconductor nanowires (NWs) have become the heart of a variety of nanosize devices in electronic and optoelectronic applications. Among these quasi-one-dimensional (1D) structures one can find field effect[1] and p-n junction[2] transistors, light-emitting diodes,[3] detectors,[4] lasers,[5] photovoltaic solar-cells,[6] medical sensors,[7,8] and so forth. In addition, semiconductor NWs offer a promising platform for fundamental research in low-dimension condensed matter physics. Noted recent examples are hybrid heterostructure devices combining a superconducting metal with a III−V semiconductor NW baring large spin−orbit coupling and Lande-g factor, namely InAs or InSb NWs.[9,10] The growing interest is associated with theoretical predictions for the emergence of Majorana fermions (MFs) in such systems[11−13] and has been further encouraged by experimental results recently published by several groups.[14−18] The MFs predicted nonabelian exchange statistics can only be tested by interchanging MFs in "T-" and "X-"shaped NW networks.[19,20] The implications of NW networks go far beyond the field of mesoscopic physics, for example, in enhancing the performance of solar cell devices[6,21,22] and creating complex biological sensors.[8,23] Thus, much effort is devoted to obtaining such networks; some growth and structural aspects related to the formation of as-grown NW intersections have already been reported.[24−26] Here, we demonstrate the growth of InAs NWs intersections formed by merging. Their crystal structure has been carefully investigated. We performed preliminary conductance measurements, which demonstrate that unavoidable structure changes at the junctions do not impose a significant potential barrier.

The InAs intersections were grown by the gold-assisted, vapor−liquid−solid (VLS) process in a high-purity molecular beam epitaxy (MBE) system. The epi-ready (001) InAs substrate, glued with In onto a (two-sided) lapped Si wafer, was initially heated in the introduction chamber to ∼180 °C for water desorption and then degassed at ∼350 °C overnight followed by an oxide blow-off with no intentional arsenic overpressure in a dedicated treatment chamber (attached to the MBE system), where a thin layer of gold (<1 nm) was subsequently evaporated. Following transfer to the growth chamber, the substrate temperature was ramped to 550 °C ripening the gold to droplets with the required size and density distribution (a combination of dissociation of the substrate into gold droplets and Oswald ripening). The wires were grown at 400 °C with group V/III ratio of ∼100, which normally provides wires free of stacking faults when grown on (111)B InAs.

It should be emphasized that the formation of our InAs junctions is random, and the yield relatively low, merely because we refrain from any patterning processes, which are incompatible with ultrahigh purity MBE growth used to form these intersections. The selectivity for the various types of junctions shown is low for exactly the same reason. This paper focuses on investigating the structure of merged NWs. Because

Received: July 12, 2013
Revised: September 10, 2013
Published: October 4, 2013

   dx.doi.org/10.1021/nl402571s | *Nano Lett.* 2013, 13, 5190−5196

we do not compromise on the purity, our hands are tight in terms of proving the versatility of the growth technique. We assume, based also on the work published by Dalacu et al.,[27] that once a processing procedure is used for introducing well-ordered gold patches for nucleating the NWs a high yield and relatively versatile process can be demonstrated based on the same principles.

The NW intersections were characterized by field emission scanning electron microscopy (FE-SEM, Zeiss Supra-55, 3 kV, working distance ~4 mm), transmission electron microscopy (TEM, Philips CM120, 120 kV; and high resolution TEM, FEI Technai F30-UT, 300 kV), and two-probe differential conductance measurements. TEM analysis was performed on NW samples that were harvested by placing a piece of the grown substrate in absolute ethanol and sonicating it for 30 s in an ultrasonic bath. The resulting suspension was dripped on carbon/colloid ion-coated lacey Cu grids. Conductance measurements were done on "K-shaped" intersections by spreading the NWs on a P^{++} doped Si substrate, capped with a 150 nm thick SiO_2 layer. Metallic contacts (Ti/Au − 5/100 nm) were evaporated on all branches of the NW junctions with an electron beam metal evaporation and standard lift-off techniques with pattern formed by an electron beam lithography system. Prior to metal evaporation, the samples were treated by an ammonium polysulfide $(NH_4)_2Sx$ solution to remove the oxide layer and passivate the NW surface with sulfur atoms. Measurements were carried out in He_3 cryostat at a temperature of 330 mK.

Figure 1a−c shows, respectively, the top, bird's eye, and side-view SEM images of a typical MBE grown on a (001) InAs surface InAs NWs. The top-view shows an exclusive growth only along one of the {011} crystal planes, parallel to the (011) facet. The bird's eye-view image shows a typical distribution of the NWs with quite rough three-dimensional bulk growth in the background. A fewer number of small droplets are buried in bulk growth, which apparently did not win the harsh competition between the bulk and NWs growth on the (001) surface; this is actually beneficial for diluting the NWs and avoiding a too high density. The side-view depicts very clearly the typical angle of 35.3° between the surface and the NWs as well as the high aspect ratio maintained for such growth.

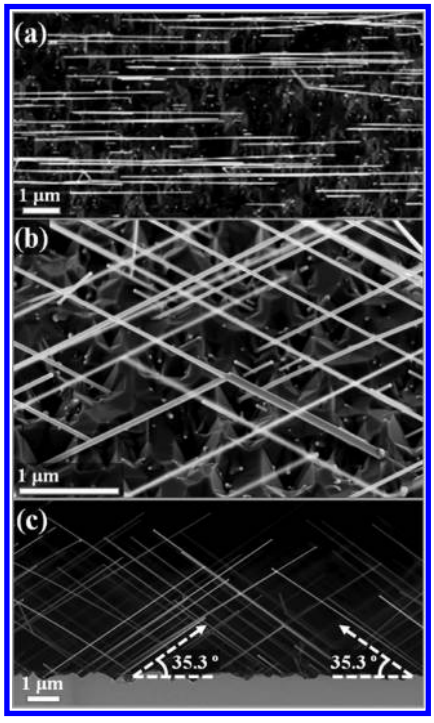

Figure 1. FE-SEM images of ⟨111⟩-oriented InAs NWs grown on (001) InAs substrate seen by (a) top-view; (b) bird's eye-view (45° tilted); and (c) side-view. (The sample edge is aligned along the (011) cleavage plane.)

Similar to the work of Dalacu et al.[27] we distinguish between two general types of NW merging; namely, tip-to-tip and tip-to-side. Figure 2 shows SEM images and schematic illustrations of

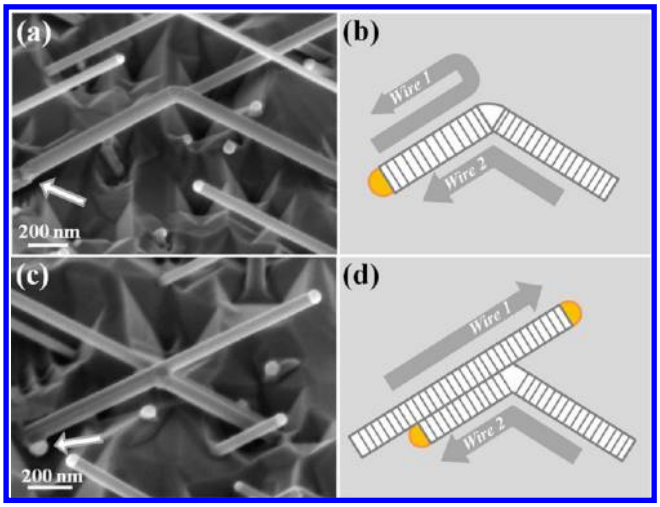

Figure 2. (a,b) and (c,d) are FE-SEM images and schematic illustrations of two InAs NWs merging tip-to-tip and tip-to-side, respectively. The arrows in panel (a) and (c) point at the position of the gold droplet after crawling down the left-hand NW.

the two most prominent NWs merging scenarios. Figure 2a,b shows an SEM image and a schematic illustration of a NW elbow formed by merging the tips of two NWs into a single gold droplet, which grows backward down the left-hand NW (marked by an arrow). The actual merging of two such tips can be seen also in the Supporting Information Figure S1. Figure 2c,d describes a "Y"-shape NW intersection, which forms after the merging of the tip of one NW with the side of another NW. Such a typical merging pattern often results in a complete joining and growth of the two NWs (see Dalacu et al.[27]).

In what follows, we look at the structural properties of the intersections formed by merging of two InAs NWs on (001) InAs substrate. The (001) surface serves as a great platform for creating merged and intersecting NWs, where the zinc blende (ZB) structure dictates four possible ⟨111⟩ growth directions, namely [111], [$\bar{1}$11], [1$\bar{1}$1] and [11$\bar{1}$], leading to a growth angle of 35.3°.[28,29] In a recent work by S. Murakami et al.,[30] Au-assisted MOCVD growth of InAs NWs on GaAs (100) and on InP (100) substrates, also exhibiting a growth angle of 35.3°, was reported. We recall that the (0001) plane in a compound material, for example, III−V, crystal of WZ structure is polar, because it consists of either cations or anions. The polarity of such surface depends on the sequence of atoms in the anion−cation pairs oriented along the [0001] direction. By analogy, the polarity of a NW is defined by the atomic sequence in the cation−anion pairs oriented along the growth direction.[31] This polarity corresponds to the electrical polarity of the unit cell of an infinitely long, [0001] oriented, WZ structure, III−V NW. Nanowires growing along the [111] and [$\bar{1}\bar{1}$1] directions have

dx.doi.org/10.1021/nl402571s | Nano Lett. 2013, 13, 5190−5196

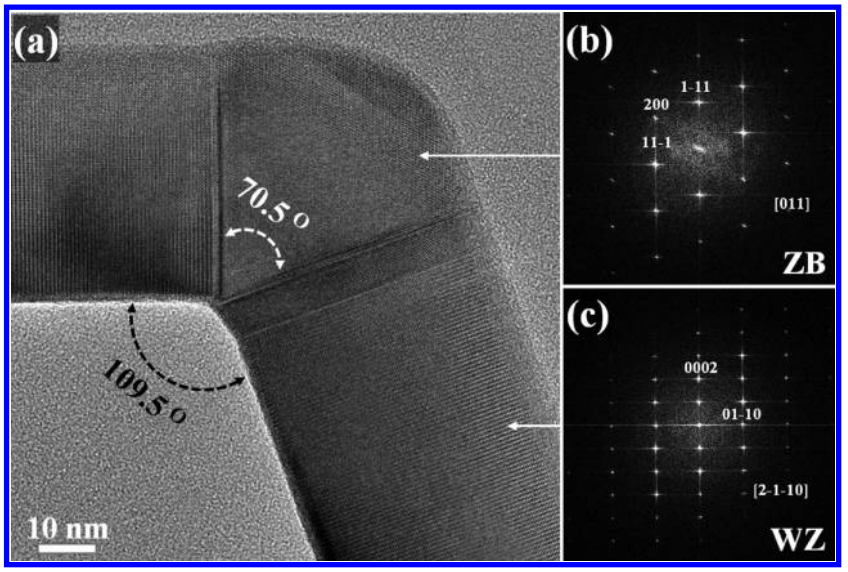

Figure 3. (a) HR-TEM image of an InAs NWs elbow resulting from a tip-to-tip merging. (b) FFT pattern of a perfect ZB and (c) FFT pattern of WZ.

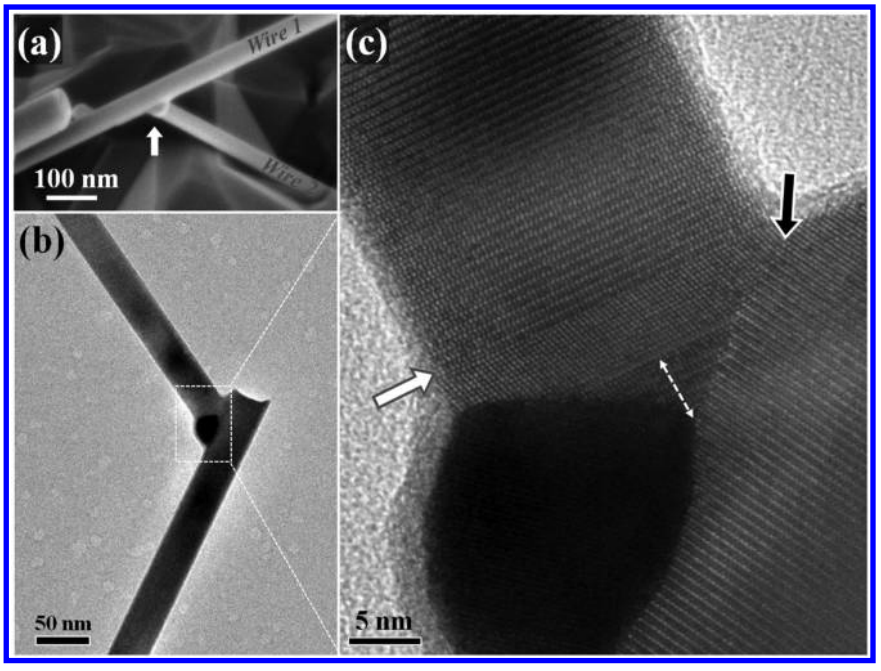

Figure 4. (a) SEM image of two InAs NWs merging tip-to-side. (b) Low-magnification TEM picture of two such merging wires. (c) HR-TEM image showing early stages of WZ NWs merging. The transition into ZB at the merging intersection is marked with a white arrow and the etched interface with a black arrow.

the same polarity that is opposite to that of the nanowires growing in the $[\bar{1}11]$ and $[1\bar{1}1]$ directions. When NWs of the same polarity merge their hexagonal cross sections encounter and the two cross-section planes form a 70.5° angle. In contrast, when NWs of opposite polarities merge, their cross-section planes form a 109.5° angle. Regardless of the crystal structure of the merging NWs, be it wurtzite (WZ) or ZB, the crystal structure of the volume filling the space between the two cross sections of the merging NWs can only be ZB. Only ZB structure, having exactly the same orientation as that of the InAs substrate, can fit the cross sections of the merging NWs for both types of polarity matching. As can be seen in Figure 1a (top view image), the NWs grow only along two directions, which are parallel to the wafer cleavage plane (namely within the same (011) plane). This means that the NWs have the same polarity. Different merging scenarios are mainly a consequence of different growth rates. NWs growing at more or less the same growth rate usually merge tip-to-tip, while merging of tip-to-side is more likely when the growth rates are different.

HR-TEM image of an InAs NWs elbow formed by merging two NWs tip-to-tip can be seen in Figure 3. Two sharp (single monolayer) transitions from WZ to ZB form the boundaries of the intersections at an angle of ~70°. It seems that the merging droplets are squeezed out of the "V"-shape intersection region while filling it with a perfectly ordered ZB structure. We speculate that when the two Au droplets merge a new interface is created and thus the ratio of droplet's volume to interface

dx.doi.org/10.1021/nl402571s | *Nano Lett.* 2013, 13, 5190−5196

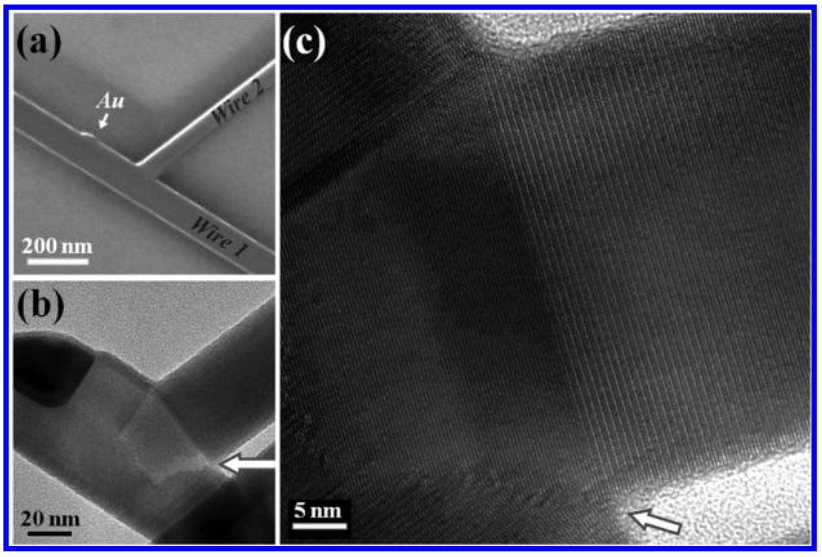

Figure 5. (a) FE-SEM image of two InAs NWs merging tip-to-side: (b) TEM and (c) HR-TEM images showing the initial stage of full merging of the hitting NW with the hit NW. The etching of the hitting NW into the hit wire can be clearly seen at the bottom of the HR-TEM image.

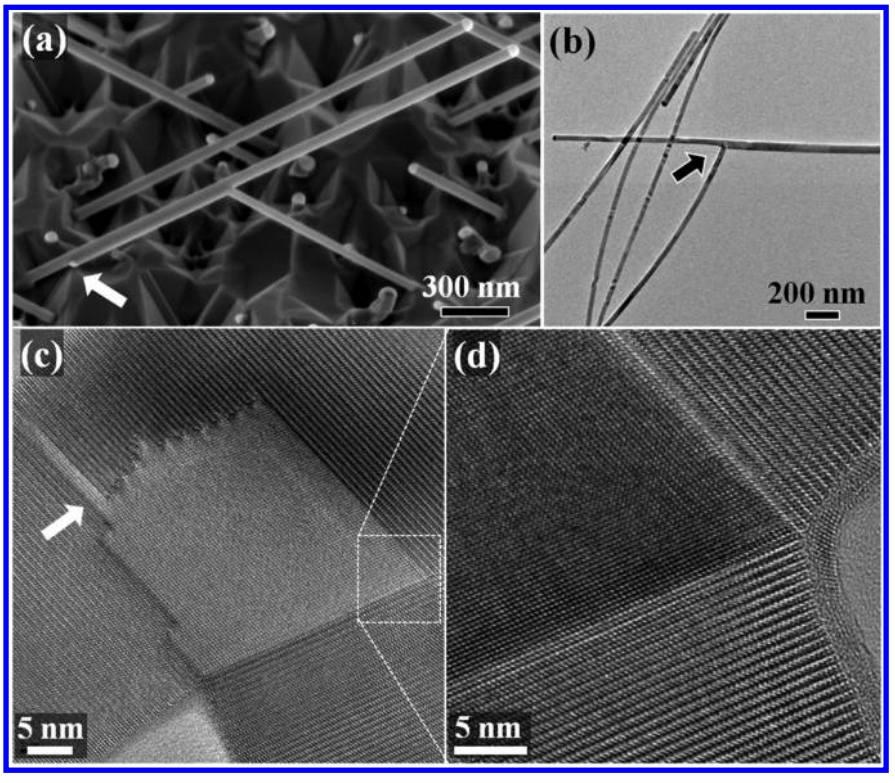

Figure 6. (a) FE-SEM and (b) TEM images of Y-shape InAs NWs merging with tip-to-side; (c) HR-TEM image of the details in the merging area, showing sharp and rough interfaces between the WZ and ZB structures. (d) HR-TEM image showing very sharp boundaries between WZ NWs and a ZB merged area at ~70° angle.

area changes and the contact angle at the three phase boundary is locally altered. Such change may induce the transition to ZB; resembling the effect of changing the arsenic supply at the termination of a NW growth. Such perfect ZB triangular intersections were recently observed by Conesa-Boj et al.[32] at the nucleation and emerging of epitaxially grown vertical "V-shaped" InAs nanomembranes on a patterned Si (001) substrate by self-assisted MBE growth.

We also studied early stages of the tip-to-side merging process (Figure 4). When the droplet barely touches the inclined NW (see arrow in Figure 4a), it squeezed into the 70.5° gap formed between the two merging NWs thanks to its low surface tension at the growth temperature. Being supersaturated, the droplet cannot etch into the hit NW, until it is fully squeezed into the triangular gap. When both WZ structures of the same polarity meet, a structural instability is induced that allows the dissociation of the hit wire (in spite of the super saturation in the droplet of the hitting NW). Here too, a sharp transition from WZ to ZB (see white arrow) can easily be seen in Figure 4c (Figure 4b shows a low-magnification TEM picture). The droplet, being captured at the new interface, manages to slightly etch into the hit wire,

dx.doi.org/10.1021/nl402571s | *Nano Lett.* 2013, 13, 5190−5196

leaving a relatively rough interface (see black arrow). Transition back into WZ occurs during the cool down process (see double side arrow). It is very possible that the gold droplet drifted along the NW during the cool down process.

In Figure 5 we show another scenario where the hitting NW crawls along the hit one. Such intersection is composed of three structural transitions: a sharp transition from WZ to ZB; a sharp transition from ZB back to WZ (the angle of ca. 70.5° between the two transitions is clearly visible), and a third prominently rough interface at the bottom of the figure (marked by an arrow). The latter results from the etching of the hitting wire into the hit wire, thus enabling conversion to ZB structure where a WZ cannot structurally fit into the intersection.

It turns out that such etching can proceed through the entire wire, during the process of converting the intersection region from WZ to ZB. Finally, Figure 6a shows an SEM image of two tip-to-side merging NWs where the hitting one is diverged to grow in the direction of the hit NW (see also in the low-magnification TEM image of a similar InAs intersection in Figure 6b). Figure 6c,d shows detailed TEM images of the intersection area with the following two important features: first, the hitting WZ NW merges in a perfect manner with the hit NW, so that the two NWs cannot be distinguished anymore beyond the ZB transition point. Moreover, a capillary penetration of the ZB transition through the entire width of the hit NW is seen in Figure 6c (marked by an arrow).

We observe that the droplet manages to etch throughout the entire diameter of the hit wire, and so the transition to ZB is extend (Figure 7a). This is extremely important since the formation of a rough transition is avoided and only three single monolayer sharp transitions form. Note that this scenario is more likely if the diameter of the hit wire is smaller than that of the hitting wire. A model depicting this type of merging can be seen in Figure 7b. It is likely that the structural transition at the merging point of the two NWs, through formation of a ZB phase, facilitates the switching of polarity. This in turn enables the crawling and elongation of the hitting NW along the hit NW, growing toward its origin in a fully epitaxial manner.

Merging of two wires tip-to-side can also result in the subsequent growth of another branch extending from the merging intersection area away from the plane determined by the two merging NWs (see Supporting Information Figure S2). Occasionally, the four arm intersections tend to have a "K"-shape where all four arms of the intersection lie in the same plane (which is an advantage for transport purposes), as shown in Figure 8a. Typically the forth arm carrying the gold droplet is shorter than the other arms. The K-shape intersections are often characterized by some parasitic growth decorating the area around the intersection. We measure the conductance through this type of wire as a representative of for a four way planar intersection. An SEM image of the device measured is shown in Figure 8b. Conductance measurements were previously reported on InAs NW intersections formed by a branching mechanism,[33] as opposed to the merging mechanism discussed here. The Si substrate was used as a back gate to control the charge carriers' density in the NWs. Two terminal conductance versus gate voltage measurements, taken at a temperature of 330 mK, are shown in Figures 8c–h for all contacts' permutations. The transition between WZ and ZB crystal structures at the intersection can be expected to introduce a potential barrier that would cause backscattering and would affect the conductance. However, the gate voltage

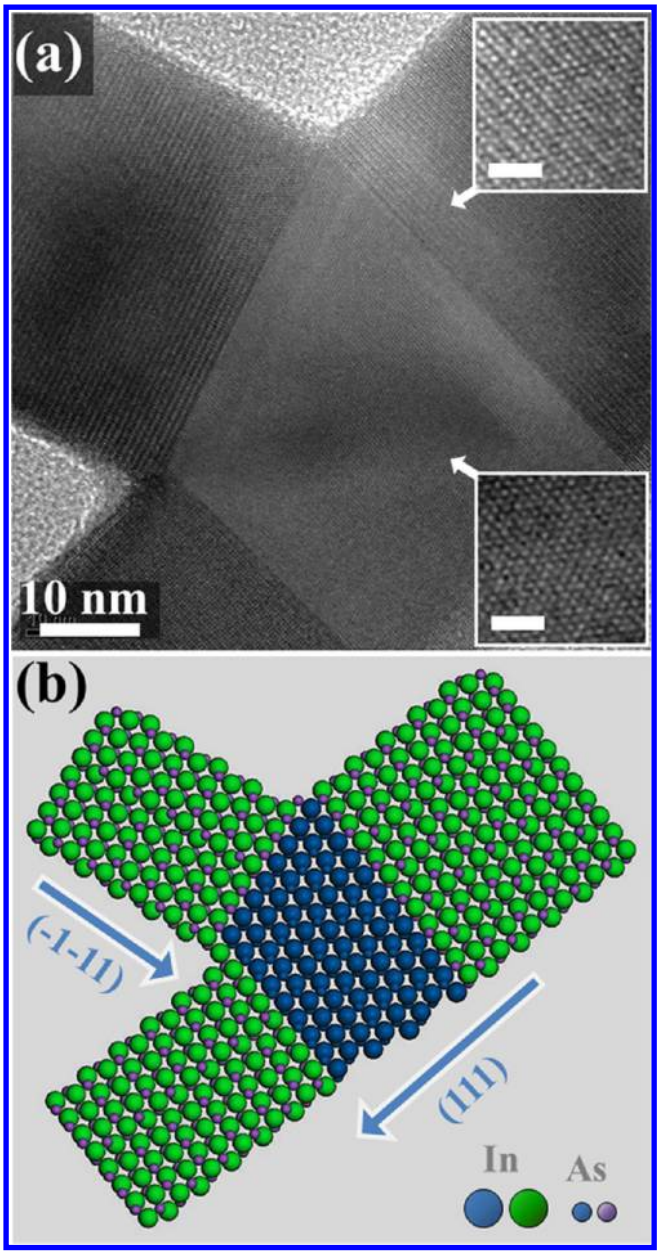

Figure 7. (a) TEM image and (b) the schematic model of two InAs NWs fully merged intersection, where the entire intersection has been transformed into ZB with three very sharp transitions; all scale bars of the in-set images are 2 nm.

dependence of the conductance resembles that of a single (straight) InAs NW grown in the same system.[34] In both cases similar conduction peaks appear as a function of gate voltage. Given the ultrahigh purity, mostly stacking faults free MBE growth of our InAs NWs (with or without an intersection) the conductance peaks are believed to be dominated by large potential barriers originating either from disorder on the surface of the wire or by the contacts. If the junction introduces additional potential barriers, they seem to be much weaker. Finally, the conductance measurements of all contacts' permutations are similar to one another. This suggests that the conductance of the junction is relatively isotropic and that all arms extending from the junction have a similar conductance.

dx.doi.org/10.1021/nl402571s | Nano Lett. 2013, 13, 5190–5196

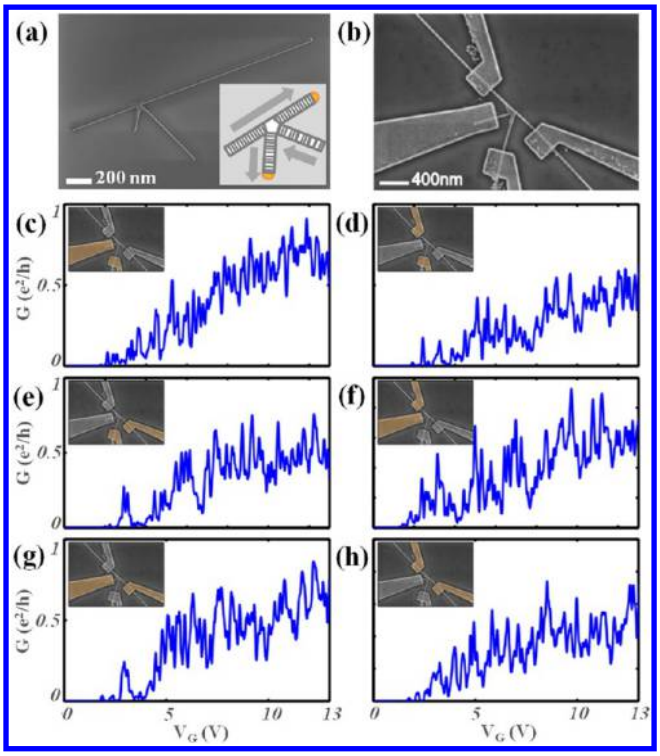

Figure 8. (a) An SEM and schematic (inset) images of the quad-arms InAs NWs (K-shape) merging of the tip-to-side type; (b) an SEM image of the device used for conductance measurements: contacts are placed on all branches of the NW junction. (c–h) Two terminal conductance versu gate voltage for all six permutations of the contacts. The SEM image of the device with the contacts (inset) used for the conductance measurement marked in orange.

In conclusion, we have demonstrated MBE growth of merged InAs NWs intersections and investigated their crystal structure and conductance. We studied the structure of the two most prominent merged intersections, namely, tip-to-tip and tip-to-side of two NWs. In both cases, a very prominent and sharp transition from WZ into ZB is a characteristic of the intersection, as expected from the structural limitations determined by the growth direction of the merging NWs. Conductance measurements show similar conductance between all NW arms across the intersection. It demonstrates that the junction does not impose an obstacle for a realization of multiple arm devices.

■ ASSOCIATED CONTENT

Supporting Information

Figure S1 shows an FE-SEM image of two InAs NWs merging tip-to-tip with the respective schematic illustration; Figure S2 depicts FE-SEM image and the atomic model of the four-arms InAs NWs intersection formed by merging of tip-to-side and an emerging of a forth NW out of the plane determined by the original NWs. Figure S2 shows a model describing such and intersection, as well as HR-TEM image of a similar intersection. This material is available free of charge via the Internet at http://pubs.acs.org.

■ AUTHOR INFORMATION

Corresponding Author

*E-mail: kjh109@weizmann.ac.il. Tel: +972-8-934-2519. Fax: +972-8-934-4128.

Author Contributions

H.S. grew the nanowires; H.S. and J.-H.K. analyzed the morphology by FE-SEM; H.S., J.-H.K., and R.P.-B. analyzed the crystal structure by TEM/HR-TEM; P.K. and R.B. supported theoretical information and atomic models; Y.R. and Y.C. measured the conductance of NW intersection under supervision of M.H.. All authors contributed to the discussions and preparation of the manuscript.

Author Contributions

⊥These authors contributed equally to this work.

Notes

The authors declare no competing financial interest.

■ ACKNOWLEDGMENTS

We are grateful to Michael Fourmansky for his unstinting technical assistance. We would also like to acknowledge partial support by the Israeli Science Foundation Grant No. 532/12 and Israeli Ministry of Science Grant No. 3-6799. We also thank to Ministry of Science and Higher Education (Poland) for partial support (Grant IP 2011013671).

■ ABBREVIATIONS

NW, nanowires; MFs, Majorana fermions; VLS, vapor–liquid–solid; MBE, molecular beam epitaxy; MOCVD, metal–organic chemical vapor deposition; FE-SEM, field emission-scanning electron microscope; TEM, transmission electron microscope; HR-TEM, high-resolution transmission electron microscope; ZB, zinc blende; WZ, wurtzite; FFT, fast Fourier transformation

■ REFERENCES

(1) Cui, Y.; Zhong, Z.; Wang, D.; Wang, W. U.; Lieber, C. M. *Nano Lett.* **2003**, *3*, 149–152.
(2) Cui, Y.; Lieber, C. M. *Science* **2001**, *291*, 851–853.
(3) Könenkamp, R.; Word, R. C.; Schlegel, C. *Appl. Phys. Lett.* **2004**, *85*, 6004–6006.
(4) Zhang, A.; You, S.; Soci, C.; Liu, Y.; Wang, D.; Lo, Y. H. *Appl. Phys. Lett.* **2008**, *93*, 121110.
(5) Huang, M, H.; Mao, S.; Feick, H.; Yan, H.; Wu, Y.; Hannes, K..; Weber, E.; Russo, R.; Yang, P. *Science* **2001**, *292*, 1897–1899.
(6) Suh, D. I.; Lee, S. Y.; Kim, T. H.; Chun, J. M.; Suh, E. K.; Yang, O. B.; Lee, S. K.. *Chem. Phys. Lett.* **2007**, *442*, 348–353.
(7) Stern, E.; Klemic, J. F.; Routenberg, D. A.; Wyrembak, P. N.; Turner-Evans, D. B.; Hamilton, A. D.; LaVan, D. A.; Fahmy, T. M.; Reed, M. A. *Nature* **2007**, *445*, 519–522.
(8) Tian, B. *Nat. Mater.* **2012**, *11*, 986–994.
(9) Wilczek, F. *Nat. Phys* **2009**, *5*, 614–618.
(10) Beenakker, C. W. J. http://arxiv.org/abs/1112, 1950.
(11) Kitaev, A. Y. *Phys.-Usp.* **2001**, *44*, 131–136.
(12) Lutchyn, R. M.; Sau, J. D.; Sarma, S. D. *Phys. Rev. Lett.* **2010**, *105*, 77001.
(13) Oreg, Y.; Refael, G.; Oppen, F. V. *Phys. Rev. Lett.* **2010**, *105*, 177002.
(14) Mourik, V.; Zuo, K.; Frolov, S. M.; Plissard, S. R.; Bakkers, P, A. M.; Kouwenhoven, L. P. *Science* **2012**, *336*, 1003–1007.
(15) Deng, M. T.; Yu, C.; Huang, G.; Larsson, M.; Caroff, P.; Xu, H. Q. *Nano Lett.* **2012**, *12*, 6414.
(16) Churchill, H. O. H.; Fatemi, V.; Grove-Rasmussen, K.; Deng, M. T.; Caroff, P.; Xu, H. Q.; Marcus, C. M. *Phys. Rev. B* **2013**, *87*, 241401.
(17) Das, A.; Ronen, Y.; Most, Y.; Oreg, Y.; Heiblum, M. *Nat. Phys.* **2012**, *8*, 887.
(18) Rokhinson, L. P.; Liu, X.; Furdyna, J. K. *Nat. Phys.* **2012**, *8*, 795.
(19) Alicea, J.; Oreg, Y.; Refael, G.; Oppen, F. V.; Fisher, M. P. A. *Nat. Phys* **2011**, *7*, 412–417.

(20) Sau, J. D.; Clarke, D. J.; Tewari, S. *Phys. Rev. B* **2011**, *84*, 094505.
(21) Cheng, C.; Fan, H. J. *Nano Today* **2012**, *7*, 327−343.
(22) Bierman, M. J.; Jin, S. *Energy Environ. Sci.* **2009**, *2*, 1050−1059.
(23) Jiang, X.; Tian, B.; Xiang, J.; Qian, F.; Zheng, G.; Wang, H.; Mai, L.; Lieber, C. M. *Proc. Natl. Acad. Sci. U.S.A.* **2011**, *108*, 12212−12216.
(24) Dick, K. A.; Deppert, K.; Karlsson, L. S.; Seifert, W.; Wallenberg, L. R.; Samuelson, L. *Nano Lett.* **2006**, *6*, 2842−2847.
(25) Wang, D.; Qian, F.; Yang, C.; Zhong, Z.; Lieber, C. M. *Nano Lett.* **2004**, *4*, 871−874.
(26) Dai, X.; Dayeh, S. A.; Veeramuthu, V.; Larrue, A.; Wang, J.; Su, H.; Soci, C. *Nano Lett.* **2011**, *11*, 4947−4952.
(27) Dalacu, D.; Kam, A.; Austing, D. G.; Poole, P. J. *Nano Lett.* **2013**, *13*, 2676−2681.
(28) Hiruma, K.; Yazawa, M.; Katsuyama, T.; Ogawa, K.; Haraguchi, K.; Koguchi, M.; Kakibayashi, H. *J. Appl. Phys.* **1995**, *77*, 447−462.
(29) Fortuna, S. A.; Li, X. *Semicond. Sci. Technol.* **2010**, *25*, 024005.
(30) Murakami, S.; Funayama, H.; Shimomura, T.; Waho, T. *Phys. Status Solidi C* **2013**, *10*, 761−764.
(31) De la Mata, M.; Magen, C.; Gazquez, J.; Utama, M. I. B.; Heiss, M.; Lopatin, S.; Furtmayr, F.; Fernández-Rojas, C. J.; Peng, B.; Morante, J. R.; Rurali, R.; Eickhoff, M.; Fontcuberta I Morral, A.; Xiong, Q.; Arbiol, J. *Nano Lett.* **2012**, *12*, 2579−2586.
(32) Conesa-Boj, S.; Russo-Averchi, E.; Dalmau-Mallorqui, A.; Trevino, J.; Pecora, E. F.; Forestiere, C.; Handin, A.; Ek, M.; Zweifel, L.; Wallenberg, L. R.; Rüffer, D.; Heiss, M.; Troadec, D.; Negro, L. D.; Caroff, P.; Fontcuberta i Morral, A. *ACS Nano* **2012**, *6*, 10982−10991.
(33) Suyatin, D. B.; Sun, J.; Fuhrer, A.; Wallin, D.; Fröberg, L. E.; Karlsson, L. S.; Maximov, I.; Wallenberg, L. R.; Samuelson, L.; Xu, H. Q. *Nano Lett.* **2008**, *8*, 1100−1104.
(34) Kretinin, A. V.; Popovitz-Biro, R.; Mahalu, D.; Shtrikman, H. *Nano Lett.* **2010**, *10*, 3439−3445.